Journal of the European Ceramic Society 16 (1996) 553–560

0955-2219(95)00159-X
0955-2219/96/$15.00

# Rietveld Refinement of the Crystal Structures of the Yttrium Silicon Oxynitrides $Y_2Si_3N_4O_3$ (N-Melilite) and $Y_4Si_2O_7N_2$ (J-Phase)

K. J. D. MacKenzie, G. J. Gainsford & M. J. Ryan

New Zealand Institute for Industrial Research and Development, P.O. Box 31-310, Lower Hutt, New Zealand

(Received 31 May 1995; revised 19 July 1995; accepted 28 August 1995)

***Abstract***

*Rietveld crystal structure refinements have been carried out on the X-ray powder patterns of synthetic N-melilite, $Y_2Si_3N_4O_3$, and J-phase, $Y_4Si_2O_7N_2$. The melilite structure of $Y_2Si_3N_4O_3$ is confirmed, in which sheets containing $Si_2O_7$ double tetrahedra are linked by Y polyhedra in which two of the eight Y–O contacts are significantly longer (2·78Å). The present data were unable to furnish unambiguous details of O/N ordering in either N-melilite or J-phase. The structure of J-phase contains either $Si_2O_5N_2$ or $Si_2O_6N$ ditetrahedral units containing N in the bridging position and arranged lengthwise along the* a*-axis. These units are linked by Y polyhedra. Of the four distinguishable Y sites, three have seven contacts with O and N atoms within 2·8Å. One of these sites also has one longer O/N contact at 2·92Å. The fourth Y site is in 6-fold coordination.*

## 1 Introduction

Yttrium oxide is commonly used to promote sintering in silicon nitride and the sialons. In these systems, it reacts to form intergranular yttrium silicon oxynitrides, of which the X-ray powder patterns and compositions of several have been reported.[1] Of these, the two phases which we have most commonly encountered in our solid-state nuclear magnetic resonance studies of silicon nitride sintering[2] have been $Y_2Si_3N_4O_3$ and $Y_4Si_2O_7N_2$. The former was detected by Rae *et al.*[3] in hot pressed $Si_3N_4$ with yttria additions, and identified as having structural similarities with the melilite minerals, of which the end members are akermanite ($Ca_2MgSi_2O_7$) and gehlenite ($Ca_2Al_2SiO_7$). The suggested structure of the new Y-containing melilite was derived from akermanite by exchanging Y for Ca, Si for Mg and four of the seven oxygens for nitrogen.[3] A satisfactory refinement of the powder data was achieved on this basis, but it was not determined whether ordering was occurring in the O/N sites, which for the purpose of the model were assumed to be occupied randomly.

No structural refinement has been published for J-phase, although Wills *et al.*[4] have suggested it to be isostructural with cuspidine ($Ca_4Si_2O_7F_2$), and indexed the powder pattern of a hot-pressed specimen on the basis of a cuspidine-like monoclinic cell.

The present structural study was made possible by the availability of essentially monophase polycrystalline samples which have been synthesised in the course of an $^{89}Y$ MAS NMR study.

## 2 Experimental

The phases were synthesised from $Si_3N_4$ (H.C. Starck GmbH & Co., Grade LC 10), $Y_2O_3$ (Sigma Chemical Co.) and, in the case of J-phase, fine $SiO_2$ (Mintech NZ Ltd, Snowsil 350). Appropriately batched mixtures were ball milled for 16 h in ethanol using $Si_3N_4$ milling media. The solvent was removed using a rotary evaporator and the powder was pressed into pellets and fired for 2 h in a flowing atmosphere of purified oxygen-free nitrogen in a graphite furnace (Thermal Technology Inc.). N-melilite was found to be extremely sensitive to the reducing potential of the furnace atmosphere, and had to be fired at 1740°C in a powder bed of BN containing a small amount of $Si_3N_4$ and $SiO_2$, contained in a loosely covered alumina pot. J-phase was readily formed at 1650°C in a BN powder bed contained in a closed graphite pot.

The O:N ratios in both materials were determined by particle-induced $\gamma$-ray emission (PIGME), in which the sample is exposed to a deuteron beam generated in an accelerator, and the $\gamma$-rays from the resulting nuclear reactions are detected and analyzed.[5] The calibration materials were $Y_2O_3$, which was used as the O standard, and $Si_3N_4$,

which was used as the N standard after correction for its residual O content. The results indicated O:N ratios of 0·7 ± 0·1 and 3·2 ± 0·1 for N-melilite and J-phase respectively, in reasonable agreement with the ratios expected from the ideal formulae (0·75 and 3·5 respectively).

Powder diffraction data for each phase were collected using a Philips PW1700 series computer-controlled diffractometer with Philips APD1700 software, a fixed 1° divergence slit, primary beam Soller slits, 0·2 mm receiving slit and graphite secondary monochromator. The pattern was collected from 10–154° $2\theta$ at 0·04° intervals using Co K$\alpha$ radiation (40 kV, 35 mA), counting for 5 s per step. The initial cell parameters for J-phase were obtained from an indexed and refined pattern from a Huber 620 114·6 mm Guinier camera used in conjunction with a KEJ Instruments LS20 microphotometer.

The data were then converted into a form suitable for Rietveld refinement by the GSAS programme suite,[6] using $\lambda$ Co K$\alpha_1$, $\alpha_2$ = 1·78896, 1·79284 Å and ratio ($\alpha_1/\alpha_2$) of 2·0. The relevant refinement variables are listed in Table 1. Beam polarisation was corrected using the value for $2\theta_m$ of 31·0°.

## 3 Results and Discussion

### 3.1 N-melilite refinement

The starting point for this refinement was the preliminary structure of Rae *et al.*[3] The structure was refined in space group P-42$_1$m using fixed O/N occupancies at the N(4)O(3) sites (see discussion below). The final cell parameters are shown in Table 1 and the refined atomic co-ordinates in Table 2, corresponding to $R_{wp}$ 0·116 and $R_p$ 0·087, where

$$R_{wp} = (\Sigma w(I_0 - I_c)^2/\Sigma w I_0^2)^{1/2}$$

$$R_p = \Sigma|I_0 - I_c|/\Sigma I_0$$

$I_0$, $I_c$ are the observed and calculated total profile intensities and $w$ are the weights (taken as $I_0^{-1}$) for each point.

The final Rietveld fitted diffraction pattern for N-melilite, all the possible Bragg reflection positions for this phase (vertical bars) and the difference between the calculated and observed intensity is shown in Fig. 1.

The calculated bond lengths and angles for this structure are shown in Tables 3 and 4 respectively.

The structure consists of $Si_2O_7$ ditetrahedra (containing Si(2)) linked together by the Si(l)

**Table 1.** Final Rietveld refinement variables for N-melilite ($Y_2Si_3O_3N_4$) and J-phase ($Y_4Si_2O_7N_2$) with $Y_2O_3$ minor phase

| | *N-melilite* | *J-phase* | *(+)* | *$Y_2O_3$* |
|---|---|---|---|---|
| Symmetry | Tetragonal | Monoclinic | — | Cubic |
| Space Group | P-42$_1$m | P2$_1$/c | — | Ia-3 |
| a, (Å) | 7·6083(1) | 7·5601(2) | — | 10·6020 |
| b, (Å) | 7·6083(1) | 10·4411(3) | — | 10·6020 |
| c, (Å) | 4·9113(1) | 10·7626(3) | — | 10·6020 |
| $\alpha$, (°) | 90 | 90 | — | 90 |
| $\beta$, (°) | 90 | 110·042(2) | — | 90 |
| $\gamma$, (°) | 90 | 90 | — | 90 |
| $\rho_{calc}$, g/cc | 4·277 | 4·592 | — | 5·034 |
| $2\theta$ zero (°) | 0·018(2) | | 0·009 | — |
| Max.shift/error | 0·03 | 0·11 | — | 0·01 |
| No. contributing reflections | 294 | 2216 | — | 286 |
| No. contributing observations | 3599 | — | 3599 | — |
| No. profile coefficients | 5 | — | 6 | — |
| No. background coefficients | 4 | — | 7 | — |
| No. soft restraints | 0 | — | 2† | — |
| No. of variables | 26 | — | 63 | — |

†Si(2)–N(1), Si(1)–O/N(6) restrained to 1·61 Å ± 0·07 Å.

**Table 2.** Final atomic co-ordinates and isotropic temperature factors in N-melilite, $Y_2Si_3O_3N_4$. Standard deviations in parentheses

| *Atom* | *Site multiplicity* | *x* | *y* | *z* | *100*U(iso)* | *N*† |
|---|---|---|---|---|---|---|
| Y | 4 | 0·1637(1) | 0·6637(1) | 0·5046(3) | 1·32(3) | 4 |
| Si(1) | 2 | 0 | 0 | 0 | 1·17(7) | 2 |
| Si(2) | 4 | 0·3591(3) | 0·8591(3) | 0·9465(7) | 1·17(7) | 4 |
| O(1) | 2 | 0 | 0·5 | 0·203(3) | 0·4(1) | 0·858 |
| N(1) | 2 | 0 | 0·5 | 0·203(3) | 0·4(1) | 1·142 |
| O(2) | 4 | 0·3553(8) | 0·8553(8) | 0·282(2) | 0·4(1) | 1·716 |
| N(2) | 4 | 0·3553(8) | 0·8553(8) | 0·282(2) | 0·4(1) | 2·284 |
| O(3) | 8 | 0·0923(7) | 0·1596(7) | 0·206(1) | 0·4(1) | 3·432 |
| N(3) | 8 | 0·0923(7) | 0·1596(7) | 0·206(1) | 0·4(1) | 4·568 |

†Total cell occupancy factor (e.g. 4 Y's per cell).

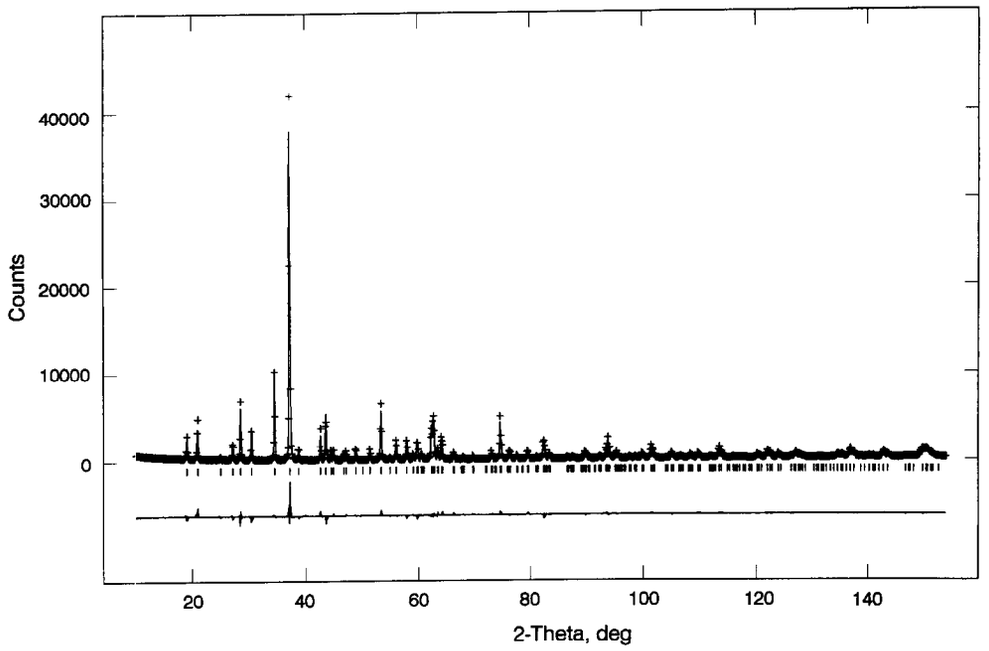


**Fig. 1.** Final diffractogram for N-melilite, $Y_2Si_3O_3N_4$.

**Table 3.** Interatomic distances in N-melilite, $Y_2Si_3O_3N_4$

| | | |
|---|---|---|
| Y–O/N(1) | | 2·303(8) Å |
| –O/N(2) | | 2·334(8) |
| –O/N(2')[a] | (2*x*) | 2·574(6) |
| –O/N(3)[b] | (2*x*) | 2·337(6) |
| Mean | | 2·411 Å |
| Y–O/N (3')[f] | (2*x*) | 2·783(6) Å |
| Si(1)–O/N(3)[c] | (4*x*) | 1·730(6) Å |
| Si(2)–O/N(1)[d] | | 1·683(6) |
| –O/N(2)[e] | | 1·648(8) |
| –O/N(3)[b] | (2*x*) | 1·733(6) |
| Mean | | 1·699 Å |

Equivalent sites are generated by symmetry operations: [a]O/N(2') *y*–1, 1–*x*, 1–*z*; 1–*y*, *x*, 1–*z*; [b]O/N(3) *y*, 1–*x*, 1–*z*; 0·5–*x*, 0·5+*y*, 1–*z*; [c]O/N(3) *x*, *y*, *z*; *y*, –*x*, –*z*; –*x*, –*y*, *z*; –*y*, *x*, *z*; [d]O/N(1) *y*, 1–*x*, 1–*z*; [e]O/N(2) *x*, *y*, 1+*z*; [f]O/N(3') –*x*, 1–*y*, *z*; 0·5–*y*, 0·5–*x*, *z*.

**Table 4.** Bond angles in N-melilite, $Y_2Si_3O_3N_4$

| | | |
|---|---|---|
| O/N(3)–Si(1)–O/N(3') | (4*x*) | 110·1(3)° |
| –O/N(3") | (2*x*) | 108·3(3) |
| Mean | | 109·5° |
| O/N(1)–Si(2)–O/N(2) | | 117·2(5)° |
| –O/N(3) | (2*x*) | 103·5(3) |
| O/N(2)–Si(2)–O/N(3) | (2*x*) | 114·9(3) |
| O/N(3)–Si(2)–O/N(3') | | 100·7(3) |
| Mean | | 109·1° |
| O/N(1)–Y–O/N(2) | | 111·9(3)° |
| –O/N(2') | (2*x*) | 74·9(3) |
| –O/N(3) | (2*x*) | 144·5(2) |
| O/N(2)–Y–O/N(2') | (2*x*) | 142·7(2) |
| –O/N(3) | (2*x*) | 78·3(3) |
| O/N(2')–Y–O/N(2") | | 74·4(3) |
| –O/N(3) | (2*x*) | 77·6(2) |
| –O/N(3') | (2*x*) | 118·4(3) |
| O/N(3')–Y–O/N(3) | | 69·7(2) |

[†]See Table 3 for definitions of symmetry operators for generating primed atoms.

tetrahedra to form sheets which lie parallel to the 001 plane of the tetragonal cell (Fig. 2). The tetrahedral sheets are linked by yttrium atoms in 8-fold co-ordination with O and N. Two of the Y–O contacts are long (>2·6 Å); these are indicated with broken lines in Fig. 2. The Y site geometry of the 6 contacts <2·6 Å approximates trigonal prismatic ($D_{3h}$) rather than octahedral, their mean bond lengths around the Y being 2·41 Å. The question of ordering on the O/N sites was examined in further detail by refining the data on the basis of three different models.

The first model, which has been adopted by Wang and Werner (personal communication) in a Rietveld refinement of Y and N melities, places all the nitrogens in one site, corresponding to the present O/N(3). Since there appears to be no steric or stoichiometric reason for adopting this simple atom distribution, a second model was tried, in which no restrictions were placed on the occupancies of the three O/N sites. On refinement, the resulting occupancies of each site produced an inconclusive stoichiometry not consistent with the analyzed O:N ratio; furthermore, no significant improvement in the refinement was obtained. In a third model, the known O/N stoichiometry was taken into account, with 3/7 of the oxygens and 4/7 of the nitrogens being allocated to each site. Again, no significant difference was observed in the refinement, indicating that the present data are not sufficiently good to differentiate between these three possibilities.

Since this work was carried out, a $^{15}N$ NMR study of N-melilite (R. K. Harris, personal communication) has provided evidence of three distinct N

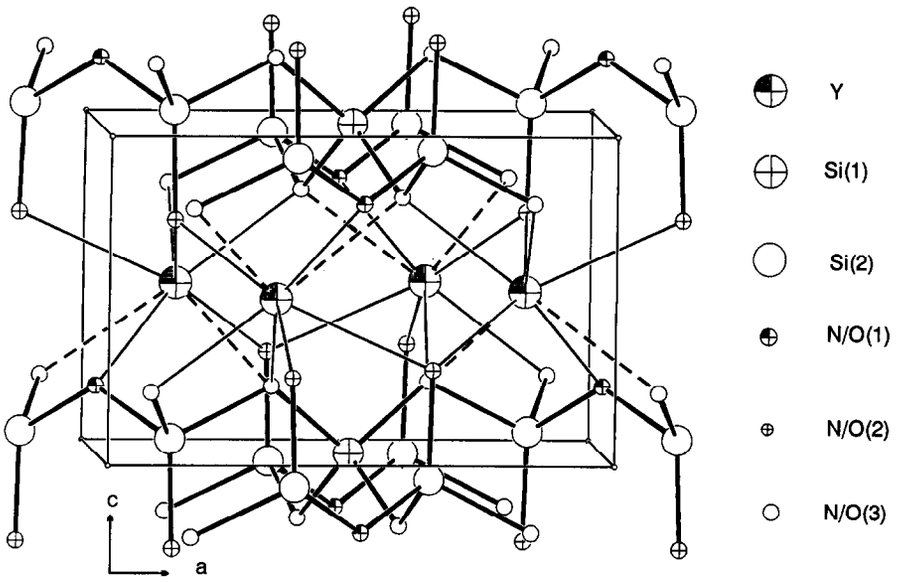


**Fig. 2.** View down *b*–axis of N-melilite cell, ORTEP II plot.[10] Dashed lines indicate Y contacts longer than 2·6 Å.

environments, suggesting an O/N ordering scheme in which O/N(1) contains only N, O/N(2) contains only O and O/N(3) contains an ordered arrangement of O and N. Since such a configuration would destroy the tetragonal symmetry, it was suggested that disorder must occur in O/N(3). The present Rietveld refinements can not discriminate between these levels of ordering; model 3 (above), in which the N and O are allowed to mix over all the O/N sites consistent with the compound stoichiometry, was adopted as the basis for the structural data of Tables 3 and 4.

### 3.2 J-phase refinement

The atom positions used as a starting point in the refinement were taken from the crystal structure of cuspidine determined by Saburi *et al.*[7] which were first transformed to conventional $P2_1/c$ co-ordinates. The original work of Wills *et al.*[4] assumed the Ca and F positions in cuspidine to be filled by Y and N respectively, but subsequent $^{29}Si$ and $^{15}N$ NMR results[8] have suggested other possible N/O ordering schemes. Hauck *et al.*[8] have observed two $^{15}N$ NMR signals in J-phase, which they assign to N in sites located in the bridging and terminal (non-bridging) positions of the Si ditetrahedral unit. This arrangement would lead to the presence of two Si environments ($SiO_3N$ and $SiO_2N_2$); the observation of only one (albeit broad) $^{29}Si$ resonance was explained in terms of the overlap of these two unresolved resonances.[8] There are, however, at least two other N/O ordering possibilities which do not involve the ditetrahedral Si unit (hereafter called 'ionic' sites). These were not discussed by Hauck *et al.*[8] but could give rise to two different $^{15}N$ resonances and one $^{29}Si$ resonance. Other possibilities include the location of N in one of the sites in the ditetrahedral unit and one of the 'ionic' sites, or in the two crystallographically distinguishable 'ionic' sites. Of these possibilities, the former may be the more reasonable, since the position of one of the observed $^{15}N$ resonances is comparable with the position found for $NSi_2$ species in other oxynitride compounds; this may correspond to the bridging site, as assigned by Hauck *et al.*[8] The present Rietveld data were therefore refined on the basis of four models: (i) that of Hauck *et al* in which one N occupies the bridging site and one N is randomly distributed over the terminal sites of the ditetrahedral units; (ii) one N occupies the bridging site of the ditetrahedral unit with the other N located randomly in the 'ionic' sites; (iii) as for model (ii), but with only one of the two distinguishable 'ionic' sites occupied by N; and (iv) the N's occupy both the 'ionic' sites.

All four models gave very similar values for $R_p$, but with a 0·2% better value obtained for models (i) and (ii) containing a bridging N. The tabulated structural data are based on model (i), although this choice is arbitrary, since the present refinements give no reason for preferring this over model (ii).

The final refined cell parameters determined for the present J-phase are listed in Table 1. During the refinement, a small amount (ca. 5%) of unreacted $Y_2O_3$ was allowed for by refining it as a second phase, using the coordinates of Hanic *et al.*[9]; the same profile function was assumed for the impurity as for the major phase because the very low concentration of the former made it impossible to determine an independent profile function. As part of the refinement process, the scale factor between the two phases was also refined. The isotropic thermal parameters for the Y, Si atoms were refined as two common values and those for the remaining atoms were fixed. The Rietveld refined diffraction pattern for this sample is shown

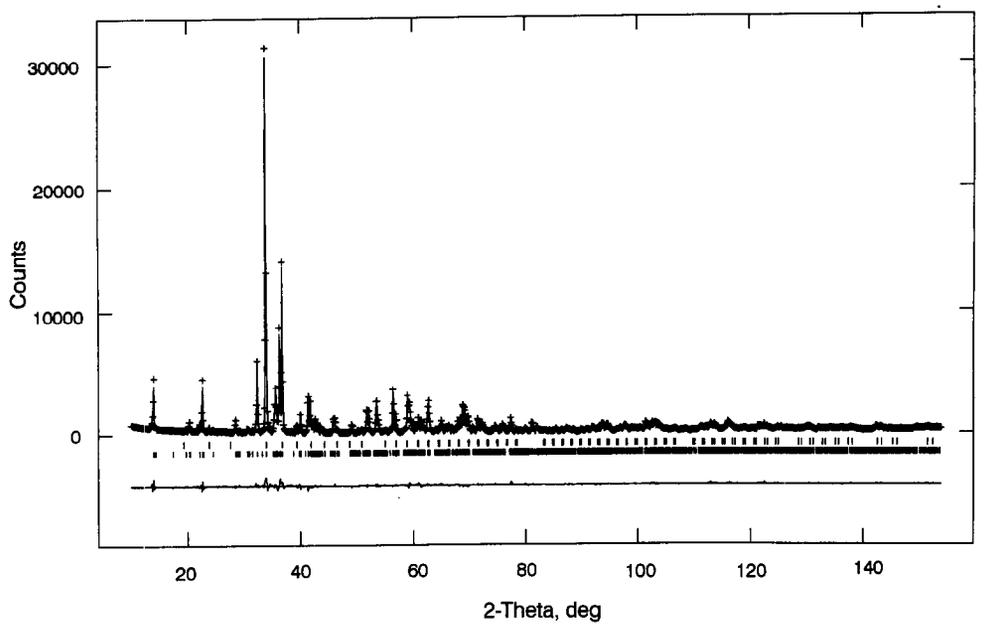


**Fig. 3.** Final diffractogram for J-phase, $Y_4Si_2O_7N_2$, with $Y_2O_3$ minor phase.

**Table 5.** Final atomic co-ordinates and isotropic temperature factors in J-phase, $Y_4Si_2O_7N_2$, and $Y_2O_3$. Standard deviations in parentheses. The multiplicities are all four in J-phase

| *Atom* | *x* | *y* | *z* | *100*(U(iso)* |
|---|---|---|---|---|
| (a) J-phase | | | | |
| Y(1) | 0·8328(8) | 0·1214(6) | 0·4290(5) | 1·14(3) |
| Y(2) | 0·3358(9) | 0·1227(6) | 0·4173(5) | 1·14(3) |
| Y(3) | 0·5281(9) | 0·4135(4) | 0·3107(4) | 1·14(3) |
| Y(4) | 0·0232(8) | 0·4024(5) | 0·2885(4) | 1·14(3) |
| Si(1) | 0·735(2) | 0·188(2) | 0·132(1) | 0·8(2) |
| Si(2) | 0·155(2) | 0·185(1) | 0·116(1) | 0·8(2) |
| N(1) | 0·939(4) | 0·240(2) | 0·109(2) | 0·8 |
| O/N(2) | 0·717(5) | 0·035(4) | 0·170(3) | 0·8 |
| O/N(3) | 0·210(5) | 0·031(4) | 0·168(3) | 0·8 |
| O/N(4) | 0·715(4) | 0·275(3) | 0·251(3) | 0·8 |
| O/N(5) | 0·282(4) | 0·265(3) | 0·244(2) | 0·8 |
| O/N(6) | 0·577(4) | 0·233(3) | –0·013(2) | 0·8 |
| O/N(7) | 0·164(4) | 0·220(3) | –0·026(2) | 0·8 |
| O(1) | 0·431(8) | 0·494(3) | 0·107(4) | 0·8 |
| O(8) | 0·918(5) | 0·519(2) | 0·097(3) | 0·8 |
| (b) $Y_2O_3$ | | | | |
| Y(1) | 0·25 | 0·25 | 0·25 | 1·0 |
| Y(2) | –0·0316(8) | 0 | 0·25 | 1·0 |
| O(1) | 0·376(5) | 0·162(3) | 0·380(7) | 1·0 |

in Fig. 3, together with all the positions of all the calculated Bragg reflections for both phases, and the difference between the calculated and observed intensities.

The final atomic co-ordinates are shown in Table 5, corresponding to $R_{wp}$ 0·101, $R_p$ (both phases) 0·075. The final weight fraction of J-phase and $Y_2O_3$ was 0·953 and 0·047 respectively. The refinement of $Y_2O_3$ minor phase gave a Y(l)–O(1) bond length of 2·13(6) Å and the three Y(2)–O bond lengths of 2·27(5) Å, 2·30(6) Å and 2·41(5) Å.

The calculated bond lengths and angles for J-phase, based on model (i) are listed in Tables 6 and 7 respectively.

**Table 6.** Interatomic distances in J-phase, $Y_4Si_2O_7N_2$

| | |
|---|---|
| Si(1)–N(1) | 1·72(3) Å |
| –O/N(2) | 1·69(4) |
| –O/N(4) | 1·61(3) |
| –O/N(6) | 1·66(2) |
| Mean | 1·67 Å |
| Si(2)–N(1") | 1·67(2) Å |
| –O/N(3) | 1·67(3) |
| –O/N(5) | 1·67(3) |
| –O/N(7) | 1·57(2) |
| Mean | 1·65 Å |
| Y(1)–N(1') | 2·38(3) Å |
| –O/N(2) | 2·78(3) |
| –O/N(4) | 2·38(3) |
| –O/N(6') | 2·73(3) |
| –O(1') | 2·33(4) |
| –O(8") | 2·27(4) |
| –O(8') | 2·25(3) |
| Mean | 2·44 Å |
| Y(2)–O/N(3) | 2·72(3) Å |
| –O/N(5) | 2·36(3) |
| –O/N(6') | 2·28(3) |
| –O/N(7') | 2·34(3) |
| –O(1") | 2·32(4) |
| –O(1') | 2·27(3) |
| –O(8) | 2·16(4) |
| Mean | 2·35 Å |
| Y(3)–O/N(2") | 2·30(4) Å |
| –O/N(3") | 2·29(4) |
| –O/N(4) | 2·31(3) |
| –O/N(5) | 2·28(3) |
| –O/N(6') | 2·38(3) |
| –O(1) | 2·20(3) |
| Mean | 2·29 Å |
| Y(4)–N(1") | 2·49(3) Å |
| –O/N(2") | 2·30(4) |
| –O/N(3"') | 2·40(3) |
| –O/N(4") | 2·63(3) |
| –O/N(5) | 2·58(3) |
| –O/N(7') | 2·30(3) |
| –O(8"') | 2·31(3) |
| Mean | 2·43 Å |

†Symmetry operations for primed atoms: N(1'), O(1'), O/N(6'), O/N(7'), O(8'): $x$, 0·5–$y$, 0·5+$z$; O(1"), O/N(2"), O/N(3"), O(8"): 1–$x$, $y$, 0·5+$x$. 0·5–$z$; N(1"), O/N(4"), O(8"'): $x$–1, $y$, $z$; O/N(3"'): –$x$, 0·5+$y$, 0·5–$z$.

**Table 7.** Bond angles in J-phase, $Y_4Si_2O_7N_2$[†]

| | | | |
|---|---|---|---|
| N(1)–Si(1)–O/N(2) | 118(2)° | O/N(6')–Y(2)–O/N(7') | 83(1)° |
| –O/N(4) | 106(2) | –O(1") | 84(1) |
| –O/N(6) | 102(2) | –O(1') | 94(1) |
| O/N(2)–Si(1)–O/N(4) | 106(2) | –O(8") | 159(1) |
| –O/N(6) | 114(2) | | |
| O/N(4)–Si(1)–O/N(6) | 111(2) | O/N(7')–Y(2)–O(1") | 166(1)° |
| Mean | 109·5° | –O(1') | 99(1) |
| | | –O(8") | 79(1) |
| N(1")–Si(2)–O/N(3) | 116(2)° | | |
| –O/N(5) | 98(2) | O(1")–Y(2)–O(1') | 78(2)° |
| –O/N(7) | 106(2) | –O(8") | 113(1) |
| O/N(3)–Si(2)–O/N(5) | 104(2) | | |
| –O/N(7) | 115(2) | O(1')–Y(2)–O(8") | 78(1)° |
| O/N(5)–Si(2)–O/N(7) | 117(2) | | |
| Mean | 109·3° | O/N(2")–Y(3)–O/N(3") | 114(1)° |
| | | –O/N(4) | 166(1) |
| N(1')–Y(1)–O/N(2) | 160(1)° | –O/N(5) | 78(1) |
| –O/N(4) | 101(1) | –O/N(6') | 100(1) |
| –O/N(6) | 62(1) | –O(1) | 83(1) |
| –O(1") | 123(1) | | |
| –O(8") | 109(1) | O/N(3")–Y(3)–O/N(4) | 78(1)° |
| –O(8') | 80(1) | –O/N(5) | 165(1) |
| | | –O/N(6') | 112(1) |
| O/N(2)–Y(1)–O/N(4) | 61(1)° | –O(1) | 84(1) |
| –O/N(6') | 115(1) | | |
| –O(1") | 71(1) | O/N(4)–Y(3)–O/N(5) | 89(1)° |
| –O(8") | 73(1) | –O/N(6') | 82(1) |
| –O(8') | 120(1) | –O(1) | 90(1) |
| O/N(4)–Y(1)–O/N(6') | 74(1)° | O/N(5)–Y(3)–O/N(6') | 74(1)° |
| –O(1") | 100(1) | –O(1) | 88(1) |
| –O(8") | 108(1) | | |
| –O(8') | 175(2) | O/N(6')–Y(3)–O(1) | 160(1)° |
| O/N(6)–Y(1)–O(1') | 74(1)° | N(1")–Y(4)–O/N(2") | 122(1)° |
| –O(8") | 171(1) | –O/N(3"') | 123(1) |
| –O(8') | 102(1) | –O/N(4") | 63(1) |
| | | –O/N(5) | 60(1) |
| O(1')–Y(1)–O(8") | 114(1)° | –O/N(7') | 102(1) |
| –O(8') | 76(1) | –O(8"') | 76(1) |
| O(8")–Y(1)–O(8') | 77(2)° | O/N(2")–Y(4)–O/N(3"') | 105(1)° |
| | | –O/N(4") | 175(1) |
| O/N(3)–Y(2)–O/N(5) | 62(1)° | –O/N(5) | 72(1) |
| –O/N(6') | 123(1) | –O/N(7') | 93(1) |
| –O/N(7') | 119(1) | –O(8"') | 82(1) |
| –O(1") | 73(1) | | |
| –O(1') | 128(1) | O/N(3"')–Y(4)–O/N(4") | 70(1)° |
| –O(8") | 76(1) | –O/N(5) | 177(1) |
| | | –O/N(7') | 106(1) |
| O/N(5)–Y(2)–O/N(6') | 74(1)° | –O(8"') | 80(1) |
| –O/N(7') | 78(1) | | |
| –O(1") | 103(1) | O/N(4")–Y(4)–O/N(5) | 113(1)° |
| –O(1') | 168(1) | –O/N(7') | 88(1) |
| –O(8") | 112(1) | –O(8"') | 97(1) |
| | | O/N(5)–Y(4)–O/N(7') | 74(1)° |
| | | –O(8"') | 99(1) |
| | | O/N(7')–Y(4)–O/N(8"') | 173(1)° |

[†]See Table 6 for definitions of symmetry operators for generating primed atoms.

The structure of J-phase according to the model whose parameters are listed in Tables 6 and 7 consists of ditetrahedral units distributed lengthwise along the *a*-axis as in Figs 4 and 5, in which the bridging atom is shown as a nitrogen N(l), with the other nitrogens distributed randomly over the terminal sites O/N(2)–O/N(7) of these $Si_2O_5N_2$ units. This represents one possible O/N ordering arrangement which is consistent with the two N sites distinguishable in the published $^{15}N$ NMR

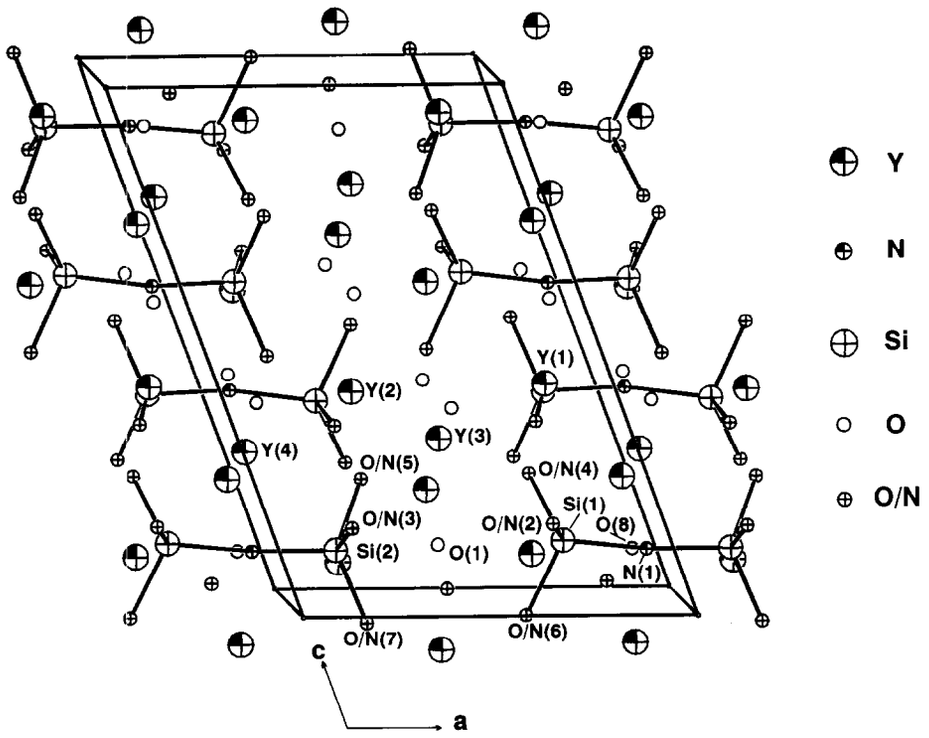


**Fig. 4.** Cell contents of J-phase, viewed down the *b*–axis, ORTEP II plot.[10] Only the Si ditetrahedral unit bonding is shown.

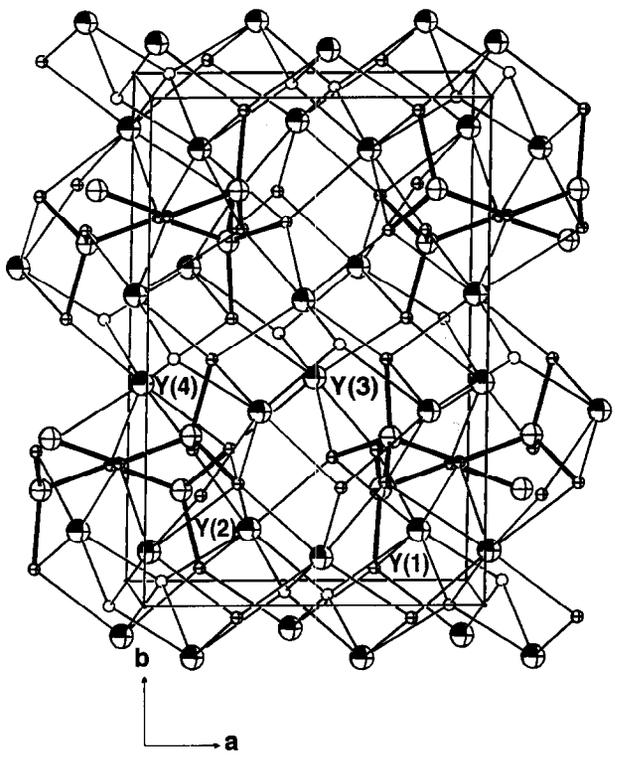


**Fig. 5.** Cell contents of J-phase, viewed down the *c*–axis, ORTEP II plot.[10] Thicker lines show the ditetrahedral unit, thinner lines show other bonding contacts. Atom symbols as for Fig. 4.

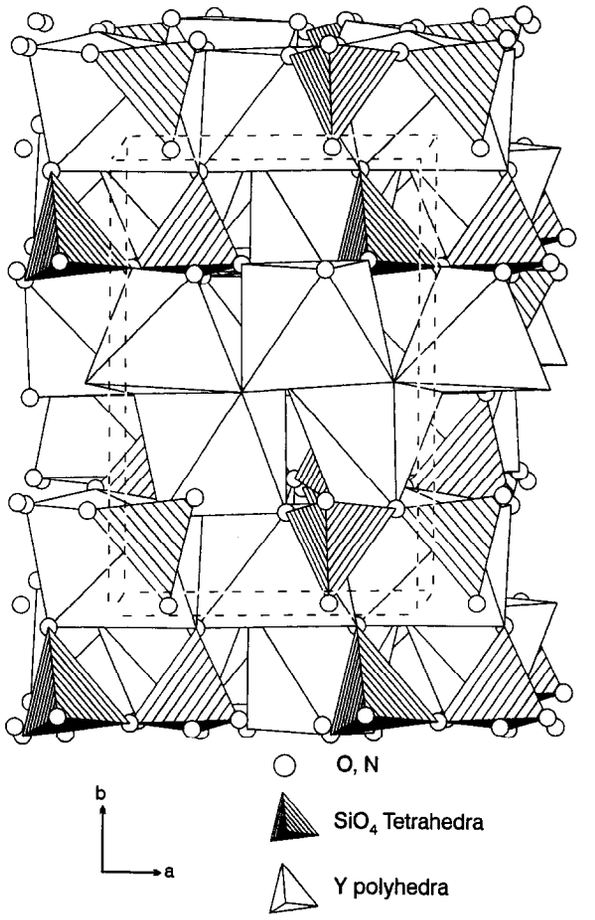


**Fig. 6.** Polyhedral coordination in J-phase, STRUPLO-90 plot.[11] Unit cell indicated by broken lines.

data[8]; the substitution of one N into the crystallographically distinguishable 'ionic' sites O(1) and O(8) cannot be ruled out by the present data. The ditetrahedral units are linked through O/N atoms with edge-shared Y polyhedra (Fig. 6) to form a corrugated wall in which four different Y environments can be identified (Tables 6 and 7). The Y polyhedra are linked together to form columns parallel to the *a*-axis, the columns forming three-dimensional networks by edge sharing. The Y–O, Y–O/N interatomic distances vary considerably;

on the basis of these contacts < 2·8 Å, the Y(1), Y(2) and Y(4) sites are all 7-co-ordinated. An additional contact with O/N(7) occurs at a distance of 2·92(3) Å from Y(1). Site Y(3) is 6-co-ordinated, with distorted octahedral geometry.

## Acknowledgement

We are indebted to Dr I. C. Vickridge for the PIGME analyses.

## References

1. Thompson, D. P., Phase relationships in Y–Si–Al–O–N ceramics. In *Tailoring Multiphase and Composite Ceramics, Materials Science Research*, Vol. 20, eds R. E. Tressler, G. L. Messing, C. G. Pantano & R. E. Newnham, Plenum, New York, 1986, pp. 79–91.
2. MacKenzie, K. J. D. & Meinhold, R. H., Role of additives in the sintering of silicon nitride: a $^{29}Si$, $^{27}Al$, $^{25}Mg$ and $^{89}Y$ MAS NMR and X-ray diffraction study. *J. Mater. Chem.*, **4** (1994) 1595–602.
3. Rae, A. W. J. M., Thompson, D. P., Pipkin, N. J. & Jack, K. H., The structure of yttrium silicon oxynitride and its role in the hot-pressing of silicon nitride with yttria additions. *Special Ceramics*, **6** (1975) 347–60.
4. Wills, R. R., Holmquist, S., Wimmer, J. M. & Cunningham, J. A., Phase relationships in the system $Si_3N_4$–$Y_2O_3$–$SiO_2$. *J. Mater. Sci.*, **11** (1976) 1305–9.
5. Vickeridge, I. C., The INS nuclear microprobe: description and applications. *NZ J. Technol.*, **1** (1985) 61–6.
6. Larson, A. C. & Von Dreele, R. B., General Structure Analysis System, Los Alamos National Laboratory, Los Alamos, NM, USA.
7. Saburi, S., Kawahara, A., Henmi, C., Kusachi, I. & Kihara, K., The refinement of the crystal structure of cuspidine. *Mineral. J.*, **8** (1977) 286–98.
8. Hauck, D. S. B., Harris, R. K., Apperley, D. C. & Thompson, D. P., Structural investigation of YAM-type yttrium silicon oxynitride by $^{15}N$ magic-angle spinning nuclear magnetic resonance. *J. Mater. Chem.*, **2** (1993) 1005–6.
9. Hanic, F., Hartmanova, M., Knab, G. G., Urusovskaya, A. A. & Bagdasarov, K. S., Real structure of undoped $Y_2O_3$ single crystals. *Acta Cryst.*, **B40** (1984) 76–82.
10. Johnson, C. K., ORTEP II. A Fortran thermal-ellipsoid plot program for crystal structure illustrations, Report ORNL 5138, (1976), Oakridge National Laboratory, Tennessee.
11. Fischer, R. X., LeLirzin, A., Kassner, D. & Rudinger, B., STRUPLO-90, version based on *J. Appl. Cryst.*, **18** (1985) 258.